

## Article

# Tribological Behavior of WS<sub>2</sub> Nanoparticles as Additives in Calcium Sulfonate Complex–Polyurea Grease

Hong Zhang <sup>1</sup> , Yimin Mo <sup>1,\*</sup>, Juncheng Lv <sup>2</sup> and Jun Wang <sup>2</sup>

<sup>1</sup> School of Mechanical and Electrical Engineering, Wuhan University of Technology, Wuhan 430070, China; hongybyb@163.com

<sup>2</sup> SAIC GM-Wuling Automobile Co., Ltd., Liuzhou 545007, China; juncheng.lv@sgmw.com.cn (J.L.); jun1.wang@sgmw.com.cn (J.W.)

\* Correspondence: moyimin@whut.edu.cn

**Abstract:** In order to improve the tribological properties of calcium sulfonate complex–polyurea grease, WS<sub>2</sub> nanoparticles were used as additives to prepare WS<sub>2</sub> calcium sulfonate complex–polyurea grease. The tribological behavior of WS<sub>2</sub> grease on the GCr15 surface was systematically studied. The results indicate that WS<sub>2</sub> nanoparticles can significantly improve the extreme pressure performance of calcium sulfonate complex–polyurea grease. When the concentration of WS<sub>2</sub> nanoparticles is 2 wt.%, the friction coefficient decreases by 14.94%, and the maximum nonseizure load PB increases by 31.41%. As the temperature increases, the friction coefficient and wear rate of WS<sub>2</sub> grease first decrease and then increase. This is mainly attributed to the adsorption and frictional chemical reaction between WS<sub>2</sub> nanoparticles and the matrix.

**Keywords:** WS<sub>2</sub> nanoparticles; calcium sulfonate complex–polyurea grease; tribological behavior; friction wear; surface analysis



**Citation:** Zhang, H.; Mo, Y.; Lv, J.; Wang, J. Tribological Behavior of WS<sub>2</sub> Nanoparticles as Additives in Calcium Sulfonate Complex–Polyurea Grease. *Lubricants* **2023**, *11*, 259.

<https://doi.org/10.3390/lubricants11060259>

Received: 22 May 2023

Revised: 4 June 2023

Accepted: 9 June 2023

Published: 12 June 2023



**Copyright:** © 2023 by the authors. Licensee MDPI, Basel, Switzerland. This article is an open access article distributed under the terms and conditions of the Creative Commons Attribution (CC BY) license (<https://creativecommons.org/licenses/by/4.0/>).

## 1. Introduction

Tungsten disulfide is one of the most common friction-reducing agents [1]. It is similar to molybdenum disulfide in structure and belongs to the disulfides of transition metals. They have high binding energy and low interlayer interaction at the interface [2], so they are inherently superlubricious. WS<sub>2</sub> nanoparticles are widely used as lubricating oil additives. Aldana P U [3] found that the use of WS<sub>2</sub> nanoparticles in polyalphaolefin (PAO) base oil can reduce wear and friction by about 70%. Wrapping WS<sub>2</sub> nanosheets with oleamine can significantly improve their solubility in base oil. Moreover, WS<sub>2</sub> adsorption film and chemical reaction film can be formed on the surface of the friction pair, which effectively improves the tribological properties of PAO at high temperature [4,5]. Inorganic fullerene (IF) WS<sub>2</sub> nanoparticles as lubricant friction modifier additives show excellent antifriction performance [6]. Their lubrication mechanism involves IF-WS<sub>2</sub> forming an adsorption film and a chemical film on the wear surface to more effectively avoid direct contact between friction pairs. Thus, the wear resistance is improved [7]. Recently, some researchers began to use WS<sub>2</sub> as a grease additive [8] and found that grease containing ionic liquid Polyaniline/tungsten disulfide composite material has better antiwear performance when lubricating steel–steel friction pairs and better tribological performance and conductivity when lubricating copper–copper friction pairs.

Nanomaterials have the advantages of strong adsorption capacity and high reactivity under the effect of a small size effect and surface interface effect [9], which provides a new idea for the development of advanced lubricating materials. Carbon nanomaterials are a kind of allotrope of carbon crystal, with a great aspect ratio and excellent mechanical, electrical, and thermal properties [10,11]. Yu et al. [12] investigated the friction properties of multi-walled carbon nanotubes. It was proved that multi-walled carbon nanotubes modified by imidazolium-based ionic liquid have excellent antiwear properties as lubricating

additives. Recent studies have shown that Mxene as an additive has better tribological performance. Compared with the base oil added with unmodified  $\text{MoS}_2\text{-Ti}_3\text{C}_2$ , amine-functionalized  $\text{MoS}_2\text{-Ti}_3\text{C}_2$  has a higher friction coefficient and wear scar diameter [13]. A composite material composed of Mxene nanosheets and some metal nanomaterials (such as Cu [14] and Ag [15]) can form a stable protective film on the worn surface, which reduces friction and wear. In addition, the alignment of fillers has a great impact on the tribological properties. The concentration and distribution of fillers in the matrix directly affect the orientation of the fillers, thus affecting the performance of their friction film and the thermal conductivity of the matrix [16].

Calcium sulfonate can not only be used as an additive in lubricating oils (friction-reducing agents [17] and detergents [18]) but also as a thickening agent for lubricating greases [19]. The calcium sulfonate complex grease (CSCG) prepared on high-alkaline calcium sulfonate has impressive overall performance. This is mainly attributed to the structure and properties of calcium sulfonate thickeners, as well as the synergistic effect of oil films and frictional chemical reaction films composed of sulfates and complex oxides [20]. Wang Z [21] et al. added organic molybdenum compounds to CSCG and found that they had very low friction coefficients (0.065) at 400 N and 500 N (maximum Hertz pressures of 3.47 GPa and 3.74 GPa, respectively). Fan X [22] studied the lubrication effect of polyalkyl cyclopentane (MAC) CSCG on TC4/steel contact under sliding and fretting conditions, finding that its antifriction performance was better than its wear resistance and that the good lubrication function of polyalkyl MAC CSCG under sliding friction mainly depended on the synergistic effect of the grease film and the chemical reaction film caused by the friction. Liu D [23] found through X-ray photoelectron spectroscopy (XPS) analysis that calcium sulfonate grease would form a boundary friction film composed of iron oxide and  $\text{FeSO}_4$ , which has good water absorption performance [24,25]. Some researchers have found that the oil film becomes thinner after CSCG absorbs water [26], but others have found that there is no significant difference in the composition of the film composed of  $\text{CaCO}_3$  and CaO whether oil is used in water or not [27]. Research has shown that there is a performance difference between CSCG and polyurea grease [28]. Wu C [29] found that nano-CuO as an additive exhibits better friction reduction performance in polyurea grease than in CSCG. Researchers have also prepared lithium complex-calcium sulfonate greases by mixing lithium composite soap and calcium sulfonate, which have good corrosion resistance for low-carbon steel due to the unique reversed micelles of calcium sulfonate and the sealing function [30].

It is true that significant progress has been made in the experimental study of the tribological properties of CSCG and  $\text{WS}_2$  nanoparticles in previous studies. However, there are still many issues that need to be studied, such as the poor sensitivity of CSCG to solid friction reducers compared with polyurea grease, and the limited research on the lubrication and friction reduction mechanism of  $\text{WS}_2$  nanoparticles in lubricating grease. In response to the above issues, this study introduced organic polyurea compounds into CSCG to prepare calcium sulfonate complex-polyurea grease (coded CSCPG) and then added different concentrations of  $\text{WS}_2$  nanoparticles to study the tribological behavior of  $\text{WS}_2$  nanoparticles as CSCPG additives on the GCr15 surface. The synergistic lubrication mechanism of the two was also explored, which can provide a theoretical and experimental basis for the design and manufacturing of high-temperature lubricating grease.

## 2. Materials and Methods

### 2.1. Materials and Samples

The preparation of CSCPG was mainly divided into the following four processes: (1) Conversion process: We added ultrahigh-alkali calcium sulfonate T106A (total base number:  $\geq 395$  mgKOH/g, Jinzhou Kangtai Lubricant Additives Co., Ltd., Jinzhou, China) and base oil PAO10 (SINOPEC Lubricant Co., Ltd., Beijing, China) to the reactor, heated to 60–80 °C, and then added dodecyl stearic acid, dodecylbenzenesulfonic acid, water, and glacial acetic acid under stirring. After sufficient stirring, the temperature was slowly

increased to 100–110 °C for the reaction for 1–2 h. (2) Composite process: we added fatty acids, calcium hydroxide aqueous solution, and boric acid aqueous solution successively to the kettle, and stirred during the reaction for 1–1.5 h. (3) Mixing process: We cooled to 65–75 °C; added diisocyanate, base oil, and cyclohexylamine to the reactor; and heated to 90–100 °C with continuous stirring for 1 h. We raised the temperature to 120–130 °C until the water in the reaction kettle was completely expelled. (4) Post-treatment: We cooled to 60 °C, added WS<sub>2</sub> nanoparticles, homogenized and grounded, and prepared a lubricating grease sample (Figure 1d). Other unlabeled chemicals were purchased from Sinopharm Chemical Agent Co., Ltd., Shanghai, China such as the analytical reagent. As shown in Figure 1a,b, the additive WS<sub>2</sub> nanoparticles (>99.9%, Suzhou Bisili New Materials Co., Ltd., Suzhou, China) exhibited a hexagonal layered structure with a relatively smooth surface, with length and width dimensions much larger than thickness dimensions, and an average particle size of 80 nm. The WS<sub>2</sub> nanoparticle sample was tested using X-ray diffraction (XRD) equipment (D8 Advance, from Bruker Company, using Cu targets, K $\alpha$  Radiation, scanning speed of 0.2 s/step, sampling interval of 0.01945° (step)), and the results are shown in Figure 1c. The position and intensity of the diffraction peak are consistent with the data of the hexagonal crystal structure of WS<sub>2</sub> (JCPDS No. 08-0237) in the joint committee on powder diffraction standards. The main peak of the sample is (002), indicating that the WS<sub>2</sub> nanoparticle sample is oriented preferentially according to the (002) crystal plane and has good crystallinity.

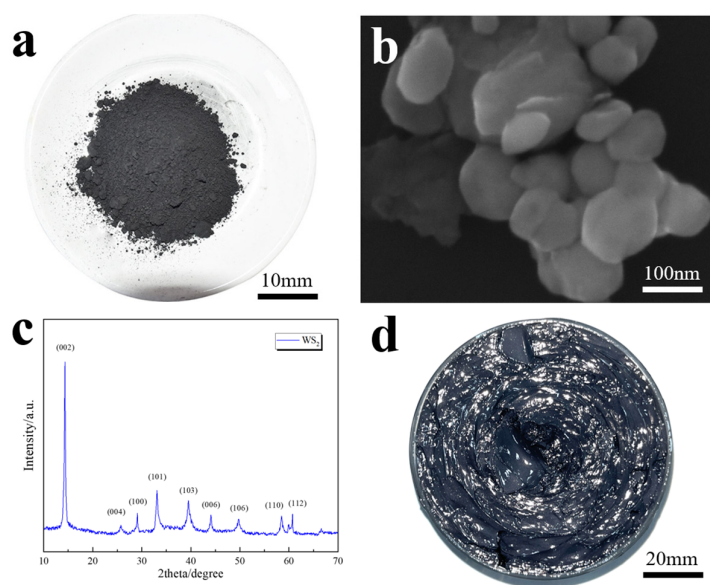


**Figure 1.** WS<sub>2</sub> nanoparticles and WS<sub>2</sub> grease samples. (a) WS<sub>2</sub> nanoparticle samples; (b) SEM microstructure of WS<sub>2</sub> nanoparticles; (c) XRD of WS<sub>2</sub> nanoparticles; (d) WS<sub>2</sub> grease samples.

## 2.2. Tribological Tests

The extreme pressure performance of the lubricating grease was evaluated using the MRS-10A four-ball friction and wear testing machine. The oil film strength PB and friction coefficient of CSCPG were tested when different concentrations of WS<sub>2</sub> nanoparticles were added to reflect the impact of WS<sub>2</sub> nanoparticles on the extreme pressure performance of the lubricating grease. GCr15 bearing steel balls with a diameter of 12.7 mm and a hardness of HRC64–66 were selected for the experiment. The tribological properties of the lubricating grease samples at different temperatures were studied using an MFT-5000 friction testing machine (Rtec, San Jose, CA, USA, Figure 2a). The friction pair samples used in the experiment included Si<sub>3</sub>N<sub>4</sub> balls (Figure 2b) and square GCr15 steel (Figure 2c). The diameter of the Si<sub>3</sub>N<sub>4</sub> ball was 6.3 mm, which was fixed on the loader and loaded vertically. The overall size of the GCr15 steel sample was 15 mm × 10 mm × 6 mm, and we polished the surface of the sample with 1200 # and 2000 # sandpaper on a polishing machine for

30 min to ensure that the surface roughness of the sample was less than  $0.05 \mu\text{m}$ . Finally, the sample was cleaned with alcohol ultrasonically for 10 min. The GCr15 steel sample was fixed on a reciprocating moving platform and moved back and forth horizontally with the moving platform. The schematic diagram of the workbench structure is shown in Figure 2d. A 3 mm thick lubricating grease sample was evenly applied to the surface of the GCr15 steel sample using a ceramic spoon. The test conditions are shown in Table 1. The real-time values of friction and load were collected by the sensors of the friction testing machine at a frequency of 100 values per second. Each sample completed three friction tests, and the average value was taken as the final test result.

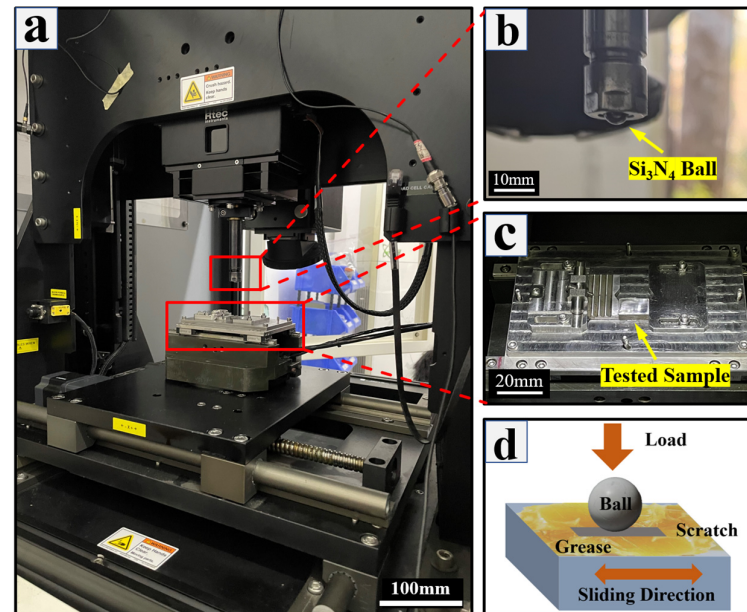


**Figure 2.** MFT-5000 friction and wear testing machine. (a) Testing machine body; (b)  $\text{Si}_3\text{N}_4$  ball; (c) Tested sample; (d) Schematic diagram of the workbench structure.

**Table 1.** Test conditions for tribological experiments.

Reciprocating Distance/mm	Reciprocating Frequency/Hz	Test Load (Fz)/N	Test Time/min	Temperature/ $^{\circ}\text{C}$
8	1	20	30	25/100/150/200

### 2.3. Surface Analysis and Characterization

After the friction test, the surface morphology of the wear marks was observed using electron probe micro-analyzer (EPMA) JAXA-8230, and the contour parameters of the wear marks were measured using a three-dimensional optical profilometer (UP-3D Rtec, San Jose, CA, USA) at different temperature tests. The middle of the wear marks on the sample was selected as the measurement position, and the contour parameters of each sample were recorded 10 times, with the average value taken as the measurement result. In addition, the wear rate ( $W, \text{mm}^3\text{n}^{-1}\text{m}^{-1}$ ) and wear amount ( $V, \text{mm}^3$ ) of the sample were analyzed using a profiler. The cross-sectional area ( $A, \text{mm}^2$ ) of the wear marks was calculated using a profiler, and each sample was measured 10 times. The average of the 10 measurements was taken as the final result. The length of wear marks ( $L, \text{mm}$ ) was obtained by calculating the circumference of the friction test trajectory. The formula for wear amount was as follows:  $V = A \cdot L$ . The formula for wear rate was as follows:  $W = V / (F \cdot S)$ , where  $F$  (N) was the load and  $S$  (m) was the total friction distance. The chemical states of elements on the worn surface were analyzed using the Thermo Scientific ESCALAB 250Xi X-ray photoelectron spectroscope. We used  $\text{Al-K}\alpha$  as the excitation source, the test energy

was 20.0 eV, the resolution was  $\pm 0.3$  eV, and the binding energy of carbon (C1s: 284.8 eV) was used as the reference calibration.

### 3. Results and Discussion

#### 3.1. Tribological Properties of Samples

As shown in Figure 3, after adding WS<sub>2</sub> nanoparticles to CSCPG, the maximum nonseizure load PB significantly increased, and the higher the concentration of WS<sub>2</sub> nanoparticles, the greater the maximum nonseizure load PB of the lubricating grease. This indicates that WS<sub>2</sub> nanoparticles can effectively improve the oil film strength of CSCPG, thereby improving its extreme pressure performance. At the same time, the addition of WS<sub>2</sub> nanoparticles also leads to a lower friction coefficient of the lubricating grease. This trend is most evident when the WS<sub>2</sub> nanoparticle concentration reaches 2.0 wt.%. Compared with the lubricating grease without WS<sub>2</sub> nanoparticles added, the friction coefficient decreases by about 14.94%, and the maximum nonseizure load PB increases by 31.41%. When the WS<sub>2</sub> nanoparticle concentration exceeds 2.0 wt.%, the maximum nonseizure load PB remains unchanged, but the friction coefficient begins to increase, which may be related to an increase in the consistency of the lubricating grease.

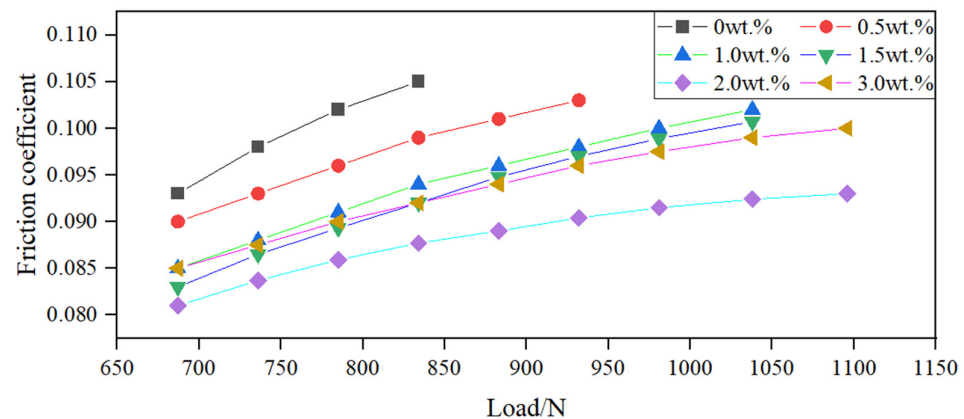


**Figure 3.** Oil film strength and friction coefficient at room temperature (25 °C) with different concentrations of WS<sub>2</sub> nanoparticles added to CSCPG.

As shown in Figure 4a, by changing the ambient temperature of the friction testing machine workbench, the friction coefficients of the lubricating grease samples were obtained at 4 temperatures: room temperature (25 °C), 100 °C, 150 °C, and 200 °C. After completing three tests at each temperature, the average value was taken to obtain the dynamic friction coefficient curve. From the trend of the curve, the friction coefficient first increases, then gradually decreases, and finally stabilizes. Among them, the time for the friction coefficient to reach stability is the shortest at 25 °C (80 s), while the other 3 temperatures (100 °C, 150 °C, and 200 °C) have a longer time to reach stability, all around 160 s. Moreover, the maximum value of the friction coefficient at these 3 temperatures is significantly higher than the friction coefficient at the stable stage, and they gradually decrease to the stable value after reaching the peak for about 100 s, but the friction coefficient at 25 °C does not show this trend. This may be due to the severe wear on the surface of the GCr15 sample during the initial stage of the experiment; the higher the viscosity of the lubricating grease, the more favorable it is for the lubricating grease to remain on the surface of the friction pair, providing better lubrication protection. The increase in temperature leads to a decrease in the viscosity of the lubricating grease sample, an increase in flowability, and easier detachment by the friction pair during the initial stage of loading, resulting in a longer time for the friction coefficient to reach stability.

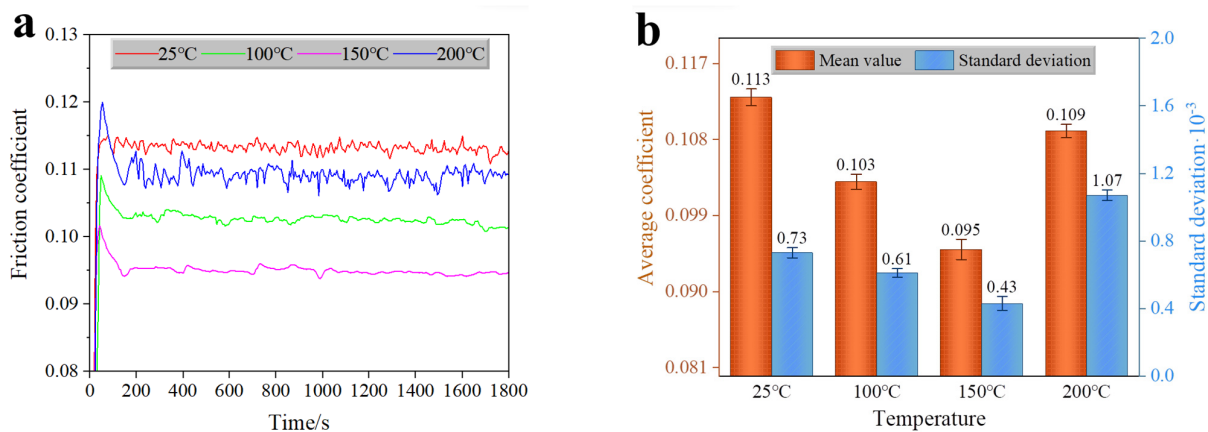


**Figure 4.** Tribological properties of  $WS_2$  grease with a concentration of 2.0 wt.% at different test temperatures. (a) Dynamic curve of friction coefficient. (b) The average and standard deviation of the friction coefficient during the stable stage.

As shown in Figure 4b, the average and standard deviation of the stable friction coefficient at different temperatures were calculated. The average friction coefficient is the highest at 25 °C, followed by the average friction coefficient at 200 °C and 100 °C, with 0.109 and 0.103, respectively. The average friction coefficient at 150 °C is the lowest, with 0.095, indicating that an increase in temperature helps to improve the friction reduction performance of  $WS_2$  grease. When the temperature is below 150 °C, the higher the temperature, the smaller the friction coefficient. Compared with room temperature (25 °C), the increase in temperature can reduce the average friction coefficient by up to 15.9%. The standard deviation of the friction coefficient in the stable stage at 150 °C is the smallest,  $0.43 \times 10^{-3}$ , indicating that the fluctuation of the friction coefficient is the smallest at this temperature. The standard deviation and average value of the friction coefficient show similar changes at 25 °C, 100 °C, and 150 °C, that is, the higher the temperature, the smaller the standard deviation, and the smaller the fluctuation of the friction coefficient. The difference is that the friction coefficient at 200 °C shows greater fluctuation than at 25 °C, which indicates that friction is more unstable at 200 °C.

From the above, it can be seen that the friction coefficient of  $WS_2$  grease on the surface of GCr15 bearing steel shows significant differences at different temperatures. Among them, the average friction coefficient is the lowest at 150 °C, and the friction coefficient is also the most stable, indicating that  $WS_2$  nanoparticles exhibit a better friction reduction effect at 150 °C. When the friction coefficient is less than 150 °C, the size and fluctuation of the friction coefficient decrease with the increase in temperature, but when the temperature rises to 200 °C, the friction coefficient actually increases and the fluctuation becomes more severe, which indicates that the antifriction effect of  $WS_2$  grease will decrease after the temperature reaches 200 °C.

### 3.2. Microstructure Characterization

As shown in Figure 5, in order to further investigate the friction and wear of  $WS_2$  grease on the surface of GCr15 bearing steel, an EPMA and a three-dimensional optical profilometer were used to observe the two-dimensional and three-dimensional morphology of the wear marks. The low-power EPMA images, 3D maps, and 2D profiles of the wear marks after different temperature tests were obtained. From the figure, it can be seen that there are obvious wear marks on the surface of the four groups of test specimens. However, the structural dimensions and surface characteristics of the wear marks vary at different temperatures. As shown in Figure 5a,d,g,j, the wear marks exhibit an obvious zoning phenomenon at all temperatures. The entire wear mark consists of two plastic deformation zones and one wear zone. The structural morphology of the two plastic deformation zones is consistent, and they are symmetrically distributed on the two edges of the wear mark

with the wear zone as the central axis. The plastic deformation zone is mainly due to the load borne by the friction pair surface exceeding the elastic limit, which cannot be restored to its original state after being squeezed and deformed. The wear zone is the result of the plastic deformation zone continuing to load; the substrate detaches from the surface, leading to wear. The plastic deformation zone has a smooth surface due to the absence of matrix detachment, while the wear zone has obvious peeling and pits. As the temperature increases, the matrix damage in the wear zone becomes more severe. When the temperature reaches 200 °C, there are obvious discontinuous pits on the surface of the worn surface (Figure 5j). As shown in Figure 5c,f,i,l, the higher the temperature, the sharper the peaks and deeper the valleys in the wear zone, and the greater the average depth of the wear marks (Figure 6a). Compared with room temperature (25 °C), the profile of the wear marks is the roughest at 200 °C, and the average depth of the wear mark increases by 12.1%. This indicates that the wear degree in the wear zone is mainly affected by temperature, and the wear of the friction pair matrix is more severe at higher temperatures.

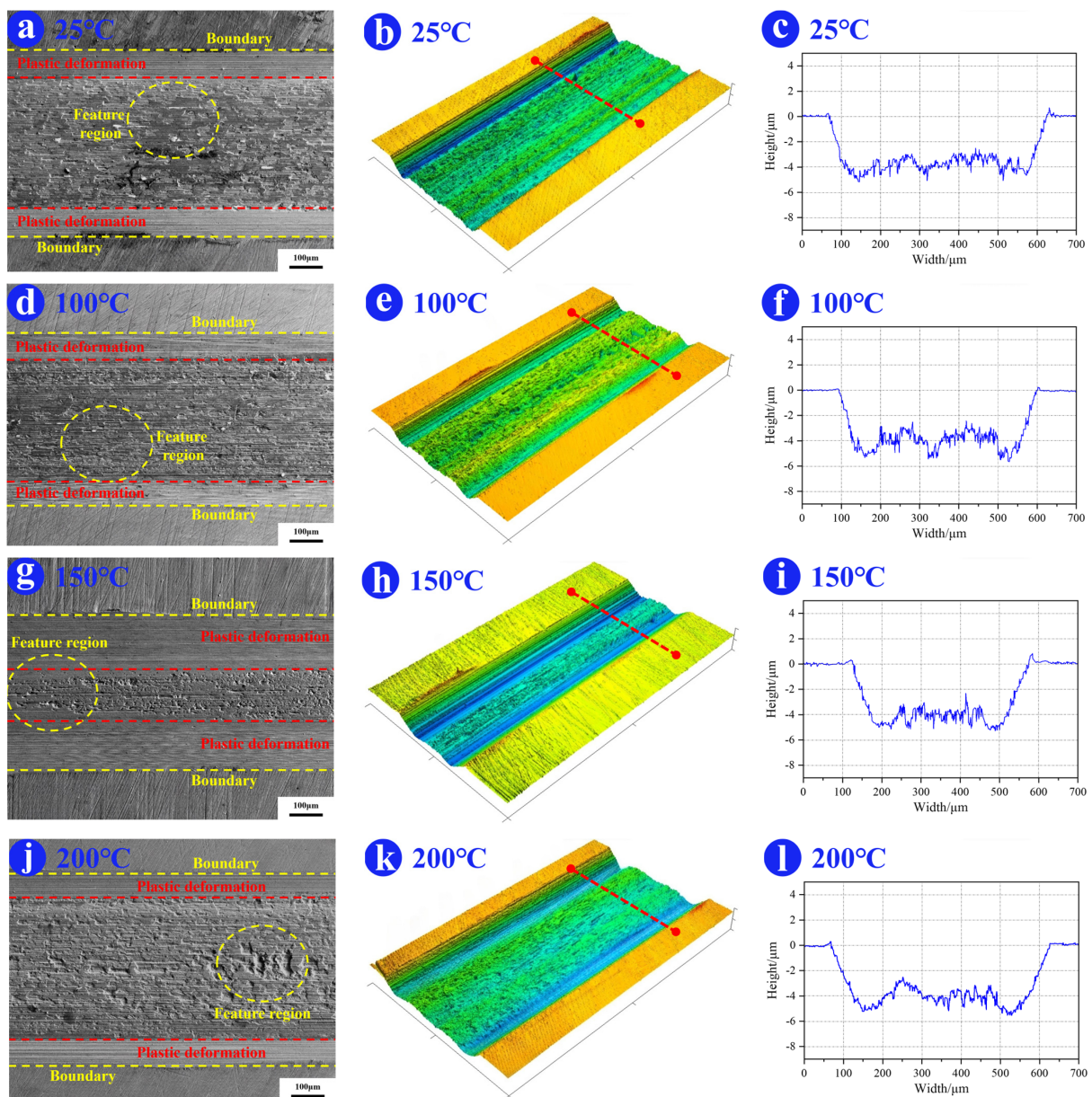


**Figure 5.** Lowmagnification EPMA images, 3D maps, and 2D profiles of wear marks at different test temperatures. (a–c) 25 °C; (d–f) 100 °C; (g–i) 150 °C; (j–l) 200 °C.

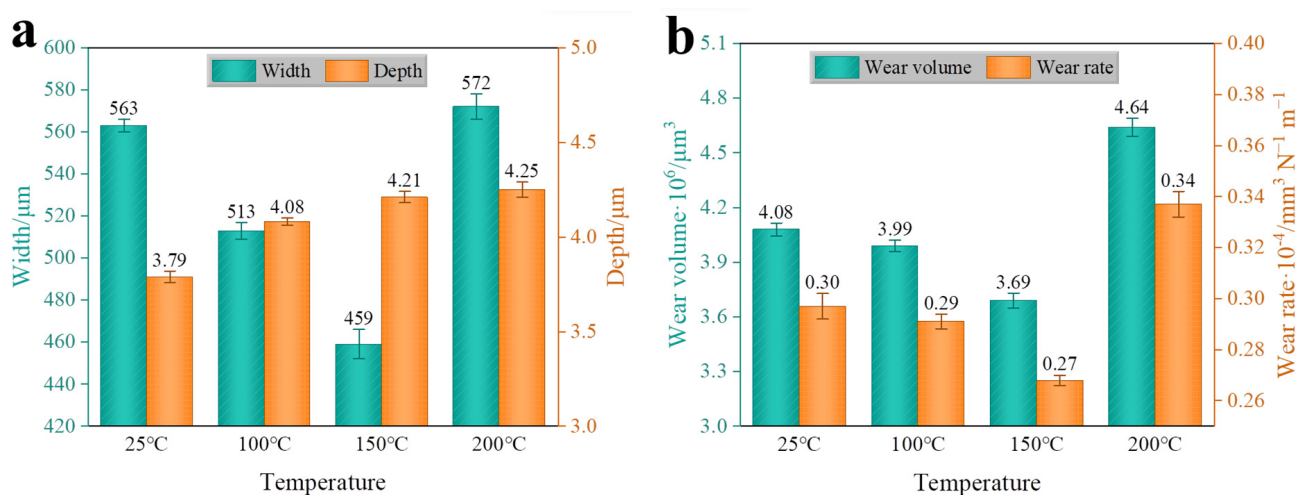


**Figure 6.** Wear performance of wear marks under different temperature tests. (a) The width and depth of wear marks. (b) Wear volume and wear rate of wear marks.

As shown in Figure 6a, the width of the wear marks and the friction coefficient exhibit a similar trend, which first decreases and then increases with the increase in temperature. At 150 °C, the width of the wear marks was the smallest, at 459 μm, and compared with 25 °C, decreased by 18.5%, while the width of the wear marks reached its maximum at 200 °C and increased by 1.6% compared with 25 °C. It is worth noting that the width of the plastic deformation zone accounts for more than 50% of the entire wear marks at 150 °C, while the proportion of the plastic deformation zone at other temperatures is much smaller than this value, which is important for the lowest friction coefficient displayed at this temperature. The possible reason is that WS<sub>2</sub> grease provides strong lubrication bearing capacity in the plastic deformation zone at 150 °C, resulting in wear occurring only in a small range.

As shown in Figure 6b, as the temperature increases, the wear volume and wear rate of the wear marks first decrease and then increase, reaching the minimum at 150 °C. Compared with 25 °C, the wear volume of the wear marks increased by 13.7% and the wear rate increased by 13.3% at 200 °C. This indicates that the wear resistance is not completely positively correlated with temperature but first improves and then decreases with the increase in temperature. When the temperature reaches 200 °C, the wear resistance actually decreases, even more than at room temperature.

As shown in Figure 7, representative characteristic areas (Figure 5a,d,g,j) within the wear zone were further magnified and observed. It can be more clearly seen that the wear on the surface of the wear marks is relatively mild at lower temperatures (25 °C and 100 °C), mainly manifested as furrows along the sliding direction and some shallow peeling pits, with a large amount of wear debris scattered on the substrate surface. The plow groove is mainly generated by the microcutting action of peeling wear debris along the sliding direction, while wear debris is mainly the product of oxidation wear on the friction surface. They detach from the substrate during continuous reciprocating sliding, causing secondary damage to the surface between the friction pairs. At higher temperatures (150 °C and 200 °C), the surface damage of the wear marks becomes severe, with fewer furrows and wear debris compared with room temperature (25 °C). The surface damage manifests more as larger and deeper peeling pits. At 150 °C, the peeling pits mainly show continuous shallow grooves along the sliding direction, while at 200 °C they show discontinuous and irregular grooves.

It is not difficult to see that the surface damage is mainly in the form of flakes at 25 °C and 100 °C, while it is in the form of blocks at high temperatures. It is speculated that the chemical reaction on the surface of the friction pair is weaker at low temperatures, and there is mainly slight oxidation wear and abrasive wear. WS<sub>2</sub> nanoparticles enter the friction pair surface and pits with the lubricating grease, providing effective lubrication protection for

the friction pair surface and preventing further deterioration of surface damage. As the temperature increases,  $WS_2$  nanoparticles begin to undergo chemical reactions with the surface, and their products adhere to the surface of the friction pair. Together with  $WS_2$  grease, they play a certain role in reducing friction and wear, further reducing the friction coefficient. However, when the temperature reaches 200 °C, the frictional chemical reaction becomes intense, and a large amount of surface products fall off from the substrate under the load, forming blocky pits that hinder reciprocating friction movement, which leads to an increase in the coefficient of friction.

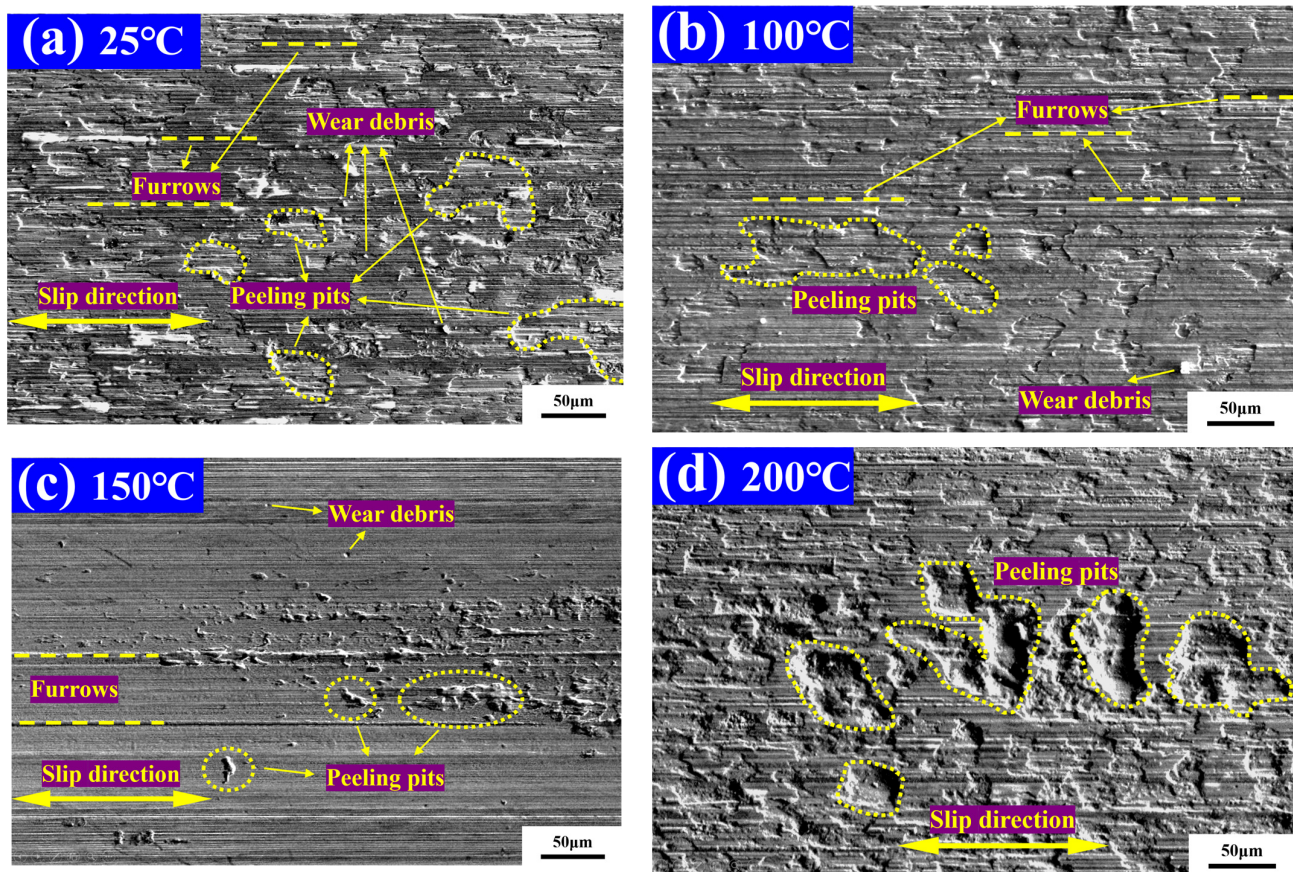


**Figure 7.** Low-magnification EPMA images of wear marks at different test temperatures. (a) 25 °C; (b) 100 °C; (c) 150 °C; (d) 200 °C.

### 3.3. XPS Analysis of the Worn Surface

As shown in Figure 8, in order to further explore the lubrication mechanism of  $WS_2$  grease on the surface of the friction pair, XPS analysis was conducted on the surface of the wear marks after the friction experiments, including Ca2p, O1s, B1s, Fe2p, C1s, N1s, S2p, and W4f. It can be seen that the residual chemical substances on the surface of the friction pair are basically the same at different temperatures, but the residual amount varies.

As shown in Figure 8a, the electronic binding energy of Ca2p at 347.4 eV and 351.5 eV may correspond to calcium carbonate and calcium oxide. Calcium carbonate comes from CSCPG, while calcium oxide comes from the decomposition of calcium carbonate. The electronic binding energy of O1s at 532.0 eV also confirms the existence of CaO (Figure 8b). As shown in Figure 8c, the electronic binding energy of B1s is attributed to borate at 193.0 eV, and element B is from CSCPG. At low temperatures, the electronic binding energy is attributed to metaborate near 192.0 eV, indicating that with the increase in temperature, metaborate is gradually transformed into borate, and the binding energy analysis of combined Ca2p may suggest that calcium metaborate is transformed into calcium borate at high temperatures (while calcium borate has been proved to have certain

extreme pressure and antiwear properties [31]). The electronic binding energy of Fe2p at 706.8 eV corresponds to iron (Figure 8d). At 710.8 eV, it indicates that Fe exists in the form of Fe<sub>2</sub>O<sub>3</sub>. At 710.5 eV and 723.5 eV, it indicates that there may be FeO and Fe<sub>3</sub>O<sub>4</sub>, which indicates that the oxidation reaction of Fe on the surface of the matrix always exists and becomes intense with the increase in temperature. The electronic binding energy of C1s is 285.1 eV and 289.5 eV, corresponding to C-C single bond and C=O double bond, respectively (Figure 8e).

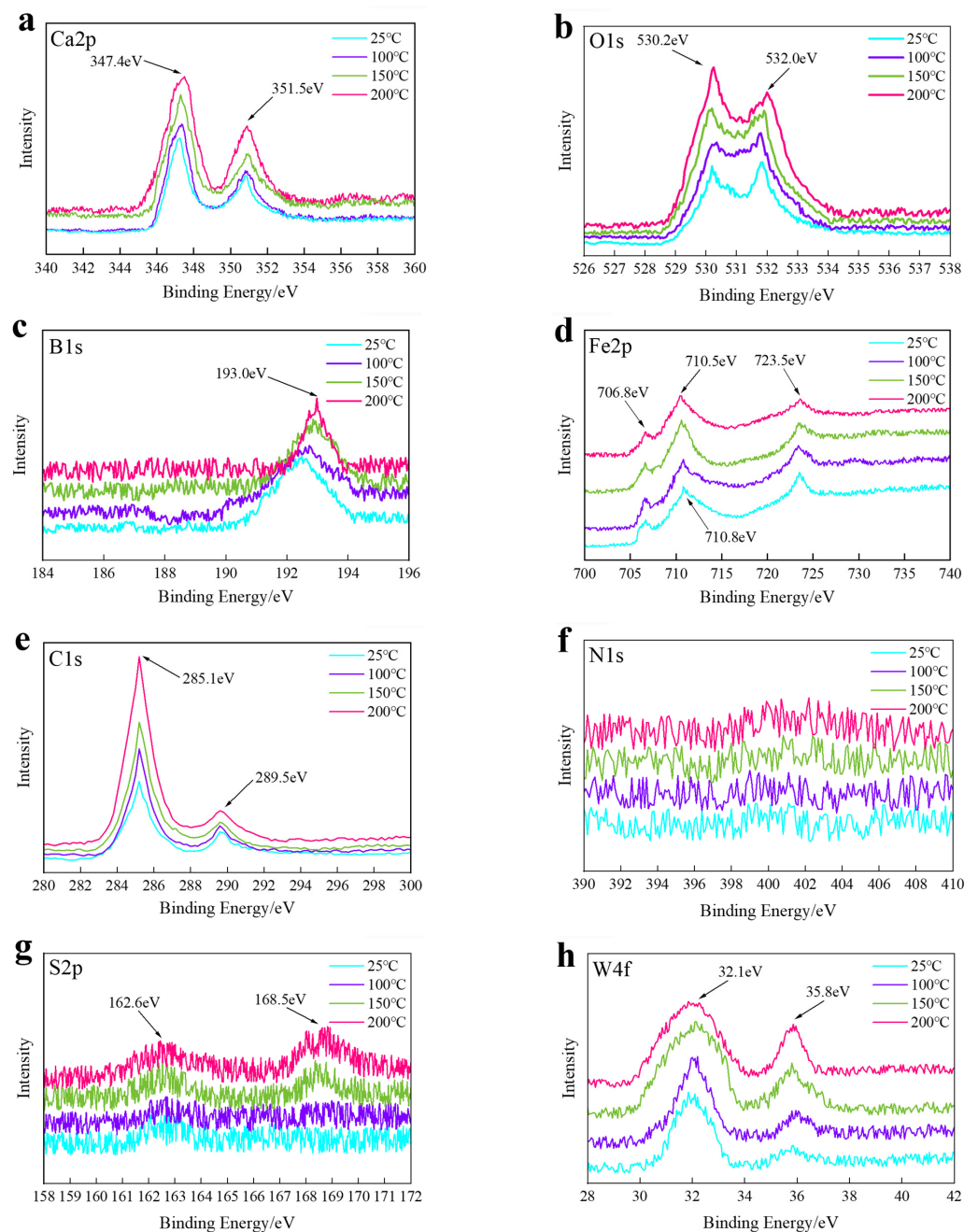


**Figure 8.** XPS of worn surface elements. (a) Ca2p; (b) O1s; (c) B1s; (d) Fe2p; (e) C1s; (f) N1s; (g) S2p; (h) W4f.

As shown in Figure 8g, the electron binding energy of S2p is mainly 162.6 eV at low temperature, corresponding to S<sup>2-</sup>, and the electron binding energy of W4f (Figure 8h) is 32.1 eV, which means that there is WS<sub>2</sub> adsorption film on the friction pair surface. The second peak of 168.5 eV gradually becomes obvious with the increase in temperature, and

the corresponding binding may be  $\text{FeSO}_4$  or  $\text{Fe}_2(\text{SO}_4)_3$ . Since the binding energy moves to the low field,  $\text{FeSO}_4$  may be generated on the friction pair surface. The electronic binding energy of W4f is mainly 32.1 eV at low temperature. With the increase in temperature, the binding energy of W4f becomes obvious at 35.8 eV. The binding energy of O1s is 530.2 eV, indicating that  $\text{WO}_3$  is generated. Due to its soft nature, it is easy to shear, which leads to low friction [32,33]. The electronic binding energy of N1s (Figure 8f) is near 400.0 eV at high temperature, which corresponds to complex N-containing compounds, while at low temperature its content is negligible.

### 3.4. Lubrication Mechanism Analysis

Based on the above results and analysis, the lubrication mechanism of  $\text{WS}_2$  nanoparticles as a CSCPG additive on the GCr15 surface can be determined. As shown in Figure 9d,  $\text{Si}_3\text{N}_4$  steel balls slide linearly on the GCr15 surface under the action of load ( $F_z$ ) and friction force ( $F_x$ ). There is a composite lubrication system between the two friction pairs (Figure 9e), which is composed of an oil film (Layer 1), an adsorption film (Layer 2), and a chemical reaction film (Layer 3). In the process of sliding friction, the surface of the material matrix (Layer 5) will deform (Figure 9b,c) to form the sub-surface damage (Layer 4). If the matrix falls off, the wear debris (Figure 9f) will also enter the composite lubrication system to participate in the friction. At room temperature, lubrication mainly relies on the oil film and adsorption film. The GCr15 substrate surface generates an iron oxide adsorption film, but the content is relatively low (Figure 8d).  $\text{CaCO}_3$  in CSCPG can decompose into a small amount of CaO, which, together with  $\text{WS}_2$  nanoparticles, forms a solid adsorption film (Figure 9g) on the friction surface. At this time, the oil film formed by the lubricating grease is thicker, so the three form a solid–oil composite lubrication system between the friction pairs, which effectively avoids mutual contact between metals and improves the antifriction performance of the lubricating grease.

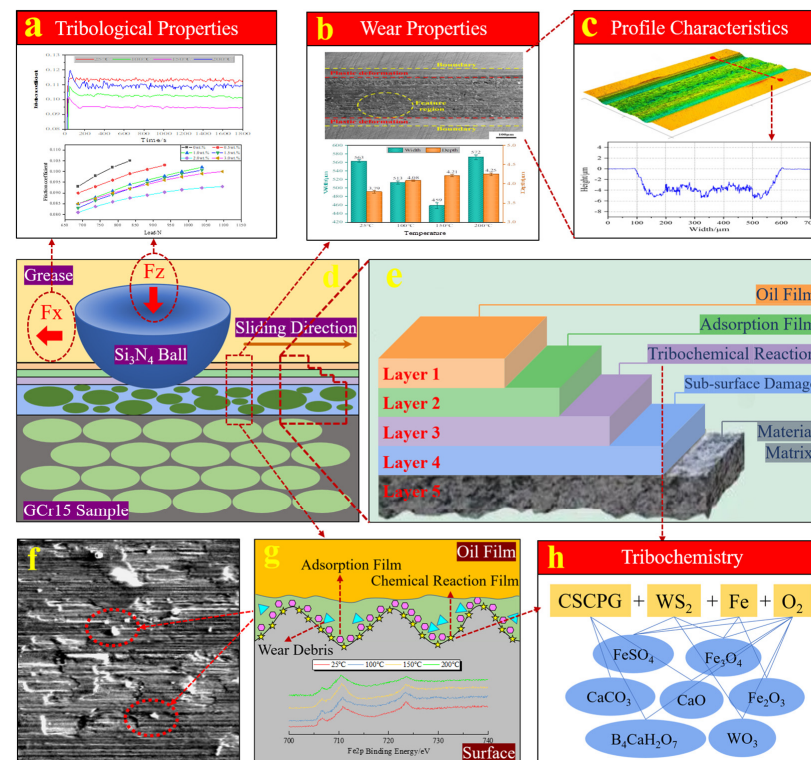


**Figure 9.** Tribological behavior and lubrication mechanism of  $\text{WS}_2$  nanoparticles in CSCPG. (a) Tribological properties; (b) Wear properties; (c) Profile characteristics; (d) Schematic diagram of friction test; (e) Composite lubrication system; (f) Wear debris; (g) Lubrication mechanism; (h) Tribochemistry.

With the increase in temperature, the viscosity of the grease becomes low and the oil film begins to thin, which makes the matrix of the friction pair easier to contact with WS<sub>2</sub> nanoparticles and oxygen. WS<sub>2</sub> nanoparticles produce more chemical reactions on the friction surface, generating WO<sub>3</sub> and FeSO<sub>4</sub> (Figure 9h). At the same time, the metacalcium borate in CSCPG transforms into calcium borate. Because the newly generated WO<sub>3</sub>, FeSO<sub>4</sub>, and calcium borate have better shear properties, they can further reduce the friction coefficient on the friction pair surface. With the further increase in temperature, the frictional chemical reaction becomes very intense, and the chemical reaction film continuously falls off and regenerates under cyclic loading, which results in a large number of peeling pits and convex peaks on the substrate surface. These surface defects actually hinder the relative motion of the friction pair, resulting in an increase in the friction coefficient.

#### 4. Conclusions

Adding WS<sub>2</sub> nanoparticles to the calcium sulfonate complex–polyurea grease can improve the load-bearing capacity of the lubricating oil film and reduce the friction coefficient. When the concentration of WS<sub>2</sub> nanoparticles reaches 2.0 wt.%, compared with the grease without WS<sub>2</sub> nanoparticles added, the friction coefficient decreases by 14.94% and the maximum nonseizure load PB increases by 31.41%.

The friction coefficient and wear rate of WS<sub>2</sub> grease decrease with the increase in temperature below 150 °C but instead begin to increase after reaching 200 °C. This is attributed to the adsorption and chemical reaction of WS<sub>2</sub> nanoparticles on the surface of the friction pair. At room temperature, WS<sub>2</sub> nanoparticles can form a solid adsorption film on the friction surface, avoiding mutual contact between metals. As the temperature increases and friction heat accumulates, WS<sub>2</sub> nanoparticles begin to undergo chemical reactions on the friction surface to generate WO<sub>3</sub> and FeSO<sub>4</sub> with better shear properties, further reducing the friction coefficient. However, the higher the temperature, the more intense the chemical reaction, which leads to an increase in wear. The matrix detachment hinders the relative motion of the friction pair, causing the friction coefficient to increase.

The calcium sulfonate complex–polyurea grease itself has a certain antifriction and antiwear ability. Under boundary lubrication conditions, CaCO<sub>3</sub>, CaO, and B<sub>4</sub>CaH<sub>2</sub>O<sub>7</sub> play a certain role in protecting the friction surface. The addition of WS<sub>2</sub> nanoparticles can enhance its antiwear ability. At high temperatures, WS<sub>2</sub> will also generate a chemical reaction film with good shear performance to produce a synergistic lubrication effect with the lubricating grease.

**Author Contributions:** Conceptualization, H.Z. and Y.M.; data curation, H.Z. and Y.M.; formal analysis, H.Z.; funding acquisition, Y.M.; investigation, J.W.; methodology, H.Z. and Y.M.; project administration, J.L.; resources, J.L.; Software, H.Z.; supervision, Y.M.; validation, H.Z., J.L. and J.W.; visualization, J.W.; writing—original draft, H.Z.; writing—review and editing, Y.M. All authors have read and agreed to the published version of the manuscript.

**Funding:** This research received no external funding.

**Data Availability Statement:** The data presented in this study are available in this article.

**Conflicts of Interest:** The authors declare no conflict of interest.

#### References

1. Takahashi, A.; Takeichi, Y.; Kimura, M.; Hashimoto, K. Low Friction Mechanism Survey of Tungsten Disulfide by Using XRD, XPS, and XAFS. *Tribol. Lett.* **2021**, *69*, 84. [[CrossRef](#)]
2. Nian, J.; Chen, L.; Guo, Z.; Liu, W. Computational investigation of the lubrication behaviors of dioxides and disulfides of molybdenum and tungsten in vacuum. *Friction* **2017**, *5*, 23–31. [[CrossRef](#)]
3. Aldana, P.U.; Dassenoy, F.; Vacher, B.; Le Mogne, T.; Thiebaut, B. WS<sub>2</sub> nanoparticles anti-wear and friction reducing properties on rough surfaces in the presence of ZDDP additive. *Tribol. Int.* **2016**, *102*, 213–221. [[CrossRef](#)]

4. Jiang, Z.; Zhang, Y.; Yang, G.; Gao, C.; Yu, L.; Zhang, S.; Zhang, P. Synthesis of oil-soluble WS<sub>2</sub> nanosheets under mild condition and study of their effect on tribological properties of poly-alpha olefin under evaluated temperatures. *Tribol. Int.* **2019**, *138*, 68–78. [[CrossRef](#)]
5. Jiang, Z.; Yang, G.; Zhang, Y.; Gao, C.; Ma, J.; Zhang, S.; Zhang, P. Facile method preparation of oil-soluble tungsten disulfide nanosheets and their tribological properties over a wide temperature range. *Tribol. Int.* **2019**, *135*, 287–295. [[CrossRef](#)]
6. Gullac, B.; Akalin, O. Frictional Characteristics of IF-WS<sub>2</sub> Nanoparticles in Simulated Engine Conditions. *Tribol. Trans.* **2010**, *53*, 939–947. [[CrossRef](#)]
7. Chen, W.; Thummavichai, K.; Chen, X.; Liu, G.; Lv, X.; Zhang, L.; Chen, D.; Tiwari, S.K.; Wang, N.; Zhu, Y. Design and Evaluation the Anti-Wear Property of Inorganic Fullerene Tungsten Disulfide as Additive in PAO6 Oil. *Crystals* **2021**, *11*, 570. [[CrossRef](#)]
8. Xia, Y.; Wang, Y.; Hu, C.; Feng, X. Conductivity and tribological properties of IL-PANI/WS<sub>2</sub> composite material in lithium complex grease. *Friction* **2023**, *11*, 977–991. [[CrossRef](#)]
9. Xia, W.; Zhao, J.; Wu, H.; Jiao, S.; Zhao, X.; Zhang, X.; Xu, J.; Jiang, Z. Analysis of oil-in-water based nanolubricants with varying mass fractions of oil and TiO<sub>2</sub> nanoparticles. *Wear* **2018**, *396*, 162–171. [[CrossRef](#)]
10. Duong, H.M.; Tran, T.Q.; Kopp, R.; Myint, S.M.; Peng, L. Chapter 1—Direct Spinning of Horizontally Aligned Carbon Nanotube Fibers and Films from the Floating Catalyst Method. In *Nanotube Superfiber Materials*, 2nd ed.; Schulz, M.J., Shanov, V., Yin, Z., Cahay, M., Eds.; William Andrew Publishing: Norwich, NY, USA, 2019; pp. 3–29. [[CrossRef](#)]
11. Duong, H.M.; Myint, S.M.; Tran, T.Q.; Le, D.K. Chapter 6—Post-spinning treatments to carbon nanotube fibers. In *Carbon Nanotube Fibers and Yarns*, 1st ed.; Miao, M., Ed.; Woodhead Publishing: Cambridge, UK, 2020; pp. 103–134. [[CrossRef](#)]
12. Yu, B.; Liu, Z.; Ma, C.; Sun, J.; Liu, W.; Zhou, F. Ionic liquid modified multi-walled carbon nanotubes as lubricant additive. *Tribol. Int.* **2015**, *81*, 38–42. [[CrossRef](#)]
13. Markandan, K.; Nagarajan, T.; Walvekar, R.; Chaudhary, V.; Khalid, M. Enhanced Tribological Behaviour of Hybrid MoS<sub>2</sub>@Ti<sub>3</sub>C<sub>2</sub> MXene as an Effective Anti-Friction Additive in Gasoline Engine Oil. *Lubricants* **2023**, *11*, 47. [[CrossRef](#)]
14. Cui, Y.; Xue, S.; Chen, X.; Bai, W.; Liu, S.; Ye, Q.; Zhou, F. Fabrication of two-dimensional MXene nanosheets loading Cu nanoparticles as lubricant additives for friction and wear reduction. *Tribol. Int.* **2022**, *176*, 107934. [[CrossRef](#)]
15. Zhou, Y.; Liu, M.; Wang, Y.; Yuan, J.; Men, X. Significance of constructed MXene@Ag hybrids for enhancing the mechanical and tribological performance of epoxy composites. *Tribol. Int.* **2022**, *165*, 107328. [[CrossRef](#)]
16. Chen, Y.; Zhang, J.; Wang, L.; Tian, Q.; Wu, J.; Li, P.; Chen, A.; Huang, S.; Lei, C. Tribological behavior of carbon-fiber-reinforced polymer with highly oriented graphite nanoplatelets. *Tribol. Int.* **2023**, *186*, 108577. [[CrossRef](#)]
17. Liu, D.; Zhang, M.; Zhao, G.; Wang, X. Tribological Behavior of Amorphous and Crystalline Overbased Calcium Sulfonate as Additives in Lithium Complex Grease. *Tribol. Lett.* **2012**, *45*, 265–273. [[CrossRef](#)]
18. Buyanovskii, I.A.; Lashkhi, V.L.; Samusenko, V.D.; Dotsenko, A.I. Tribological Characteristics of Calcium Sulfonates as Detergents for Engine Oils. *J. Frict. Wear.* **2017**, *38*, 115–120. [[CrossRef](#)]
19. Bedekar II, V.; Mistry, K.; Voothaluru, R.; Qu, J.; Poplawsky, J. Atomistic investigation of calcium sulfonate and lithium complex grease tribofilms under severe sliding conditions. *CIRP Ann.-Manuf. Technol.* **2022**, *71*, 497–500. [[CrossRef](#)]
20. Fan, X.; Li, W.; Li, H.; Zhu, M.; Xia, Y.; Wang, J. Probing the effect of thickener on tribological properties of lubricating greases. *Tribol. Int.* **2018**, *118*, 128–139. [[CrossRef](#)]
21. Wang, Z.; Xia, Y.; Liu, Z. The rheological and tribological properties of calcium sulfonate complex greases. *Friction* **2015**, *3*, 28–35. [[CrossRef](#)]
22. Fan, X.; Fu, H.; Li, W.; Zhu, M. Exploring Lubrication Function of MACs Greases for TC4 Alloy under Sliding and Fretting Conditions. *Tribol. Lett.* **2018**, *66*, 135. [[CrossRef](#)]
23. Liu, D.; Zhao, G.; Wang, X. Tribological Performance of Lubricating Greases Based on Calcium Carbonate Polymorphs Under the Boundary Lubrication Condition. *Tribol. Lett.* **2012**, *47*, 183–194. [[CrossRef](#)]
24. Bosman, R.; Lugt, P.M. The Microstructure of Calcium Sulfonate Complex Lubricating Grease and Its Change in the Presence of Water. *Tribol. Trans.* **2018**, *61*, 842–849. [[CrossRef](#)]
25. Zhou, Y.; Bosman, R.; Lugt, P.M. On the Shear Stability of Dry and Water-Contaminated Calcium Sulfonate Complex Lubricating Greases. *Tribol. Trans.* **2019**, *62*, 626–634. [[CrossRef](#)]
26. Cyriac, F.; Lugt, P.M.; Bosman, R.; Venner, C.H. Impact of Water on EHL Film Thickness of Lubricating Greases in Rolling Point Contacts. *Tribol. Lett.* **2016**, *61*, 23. [[CrossRef](#)]
27. Sun, L.; Ma, R.; Zhao, Q.; Zhao, G.; Wang, X. The Impact of Water on the Tribological Behavior of Lubricating Grease Based on Calcium Carbonate Polymorphs. *Lubricants* **2022**, *10*, 188. [[CrossRef](#)]
28. Gao, Y.; Ge, X.; Wen, Z.; Xia, Y. Comparison Friction and Wear Properties of Overbased Calcium Sulfonate Complex Grease and Polyurea Grease. *Adv. Mater. Res.* **2013**, *734–737*, 2484. [[CrossRef](#)]
29. Wu, C.; Xiong, R.; Ni, J.; Yao, L.; Chen, L.; Li, X. Effects of CuO nanoparticles on friction and vibration behaviors of grease on rolling bearing. *Tribol. Int.* **2020**, *152*, 106552. [[CrossRef](#)]
30. Ren, G.; Zhang, P.; Li, W.; Fan, X.; Zhang, L.; Li, H.; Zhu, M. Probing the Synergy of Blended Lithium Complex Soap and Calcium Sulfonate Towards Good Lubrication and Anti-Corrosion Performance. *Tribol. Lett.* **2020**, *68*, 99. [[CrossRef](#)]
31. Yan, J.; Zeng, H.; Liu, T.; Mai, J.; Ji, H. Tribological Performance and Surface Analysis of a Borate Calcium as Additive in Lithium and Polyurea Greases. *Tribol. Trans.* **2017**, *60*, 621–628. [[CrossRef](#)]

32. Li, Z.; Meng, F.; Ding, H.; Wang, W.; Liu, Q. Preparation and Tribological Properties of Carbon-Coated WS<sub>2</sub> Nanosheets. *Materials* **2019**, *12*, 2835. [[CrossRef](#)]
33. Liu, J.; Yan, Z.; Zhang, X.; Hao, J.; Zhou, H.; Liu, W. Response Mechanism of Structure and Tribological Properties of WS<sub>2</sub>/P201 Hybrid Lubrication System Under Atomic Oxygen Irradiation. *Tribol. Trans.* **2023**, *66*, 185–192. [[CrossRef](#)]

**Disclaimer/Publisher's Note:** The statements, opinions and data contained in all publications are solely those of the individual author(s) and contributor(s) and not of MDPI and/or the editor(s). MDPI and/or the editor(s) disclaim responsibility for any injury to people or property resulting from any ideas, methods, instructions or products referred to in the content.